Rev. Adv. Mater. Sci. 30 (2012) 133-149

SYNTHESIS, CHARACTERIZATION AND APPLICATIONS OF BIMETALLIC (Au-Ag, Au-Pt, Au-Ru) ALLOY NANOPARTICLES

Afzal Shah, Latif-ur-Rahman, Rumana Qureshi and Zia-ur-Rehman

Department of Chemistry, Quaid-i-Azam University, 45320, Islamabad, Pakistan

Received: December 29, 2011

Abstract. This review article describes the preparation and characterization of bimetallic alloy nanoparticles of Au-Ag, Au-Pt, and Au-Ru. The synthetic details of monometallic nanoparticles of Au, Ag, Ru, and Pt have been given for comparison. The main objective of this review is to clearly, quantitatively, and comprehensively describe the synthesis of bimetallic alloy nanoparticles and their characterization. A number of synthetic methods have been discussed in detail to provide the reader with an extensive knowledge of controlling the nanoparticle physical characteristics (size, size distribution, morphology). For getting valuable surface information, CO adsorption studies of all the three samples have also been presented. The application of bimetallic alloy nanoparticles as electrocatalysts for direct methanol fuel cell and their ability to oxidize methyl alcohol with 60% more efficiency than multi walled carbon nanotubes supported on monometallic Pt nanoparticle catalyst has also been discussed.

1. INTRODUCTION

Alloying of metals is a way of developing new materials that have better technological usefulness than their starting substances. Alloy nanoparticles show different structural and physical properties than bulk samples [1,2]. Increase in solid solubility of alloy components with decreasing particle size is one of the prominent effects. Bimetallic nanoparticles (BMNP) have excelled monometallic nanocrystals owing to their improved electronic, optical and catalytic performances [3,4]. BMNP often improve the selectivity of metal catalyzed reactions. Moreover, the change in composition of metals provides another dimension in tailoring the properties of BMNP besides the usual size and shape manipulation.

BMNP may have random, cluster-in-cluster, core shell and alloy structures. In random structure, atoms are arranged haphazardly. One element in cluster-in-cluster type forms nanoclusters and the other acts as binder. In bulk metals, two kinds of metal elements often provide an alloy structure. Elements with similar atomic sizes form a random alloy while intermetallic alloy is formed by elements of different atomic sizes.

The oxygen reduction reaction (ORR) plays a major role in several electrochemical systems, such as fuel cells, batteries, corrosion, and biological processes [5]. Therefore, considerable attention has been focused on this reaction. Platinum is usually employed as ORR catalyst because measurable current density is obtained only in this metal due to low exchange current density and high potential. The search for more active and less expensive ORR catalysts, with greater stability than Pt has resulted in the development of several Pt alloys. In this context, it has been reported that alloying platinum with transition metals such as Fe, Ru, Co, Pt, Ag,

Corresponding author: Afzal Shah, e-mail: afzals_qau@yahoo.com

etc., enhances the electro-catalytic activity of ORR by reducing Pt-O formation [6,7]. However, such an improvement has also been attributed to various structural and electronic changes caused by alloying. Japan and Taylor have documented that shortening of Pt-Pt inter-atomic distance after alloying results in activity enhancement [8]. Beard and Ross related the increase in activity to the exposure of a more active vicinal plane on dispersed platinum particle [9]. Several researchers have explained the enhanced ORR activity on the basis of interplay between the decrease of electronic Pt d-vacancy and coordination number [9-11]. Toda and coworkers suggested that increased d-electron vacancy at a thin Pt surface layer by underlying alloy is responsible for ORR enhancing mechanism [11]. A part of the current review is devoted to the activity of Au-Ag, Au-Ru and Au-Pt, for the kinetics of ORR in acidic medium. The aim of the kinetic data analysis is to correlate the catalytic activity with electronic and structural properties of the nanoparticles [12]. Hydrogenation rate of simple olefins is increased in the presence of palladium catalysts containing 20% gold, when compared with monometallic palladium catalysis [13]. The nanoparticles are stabilized with polymers but high molecular mass polymers can reduce the catalytic properties of such particles. Hence, citrate, being relatively small in size is more likely to stabilize nanoparticles without causing hindrance during catalysis.

BMNP have wide range of applications in technologies due to additional degrees of freedom as compared to monometallic nanoparticles [14-16]. However, in spite of intensive research in size and shape manipulation of BMNP, it is still a significant challenge to control their internal structures and chemical order with sizes smaller than 5 nm [16]. The current review is mainly focused on the controlled synthesis of Au-Ag, Au-Pt, and Au-Ru nanoparticles via a chemical reduction route using citrate and thiol-stabilised gold nanoparticle seeds as a starting material. An important aspect of the article is the characterization of the particles, without which the size, monodispersity and shape characteristics could not be determined.

2. SYNTHESIS

2.1. Synthesis of monometallic nanoparticles

$H_2PtCl_6.6H_2O$, $HAuCl_4.33H_2O$, $AgNO_3$, Dodecylamine, 1-dodecanethiol, sodium borohydride, sodium citrate, ethanol, toluene, and de-ionized water are used for the synthesis of Au, Ag, and Pt nanoparticles [12]. 0.8 mL of 4 mM aqueous sodium citrate solution is added to 10 mL of 1 mM aqueous $AuCl_3$ solution. Under vigorous stirring, 0.75 mL of 112 mM aqueous $NaBH_4$ solution is introduced drop wise to prepare Au hydrosol in which sodium citrate acts as a stabilizer. The molar ratio of $NaBH_4$ to $AuCl_3$ is kept constant to ensure the reduction of Au to zero valence state. The Ru hydrosol is also left to stand for 4 hours to complete the reduction reaction. The hydrosol is then mixed with 10 mL of ethanol containing 100 μL of dodecylamine and the mixture is stirred for 2 minutes. 5 mL of toluene is added with stirring continued for 3 more minutes. Dodecylamine-stabilized Au nanoparticles are rapidly extracted from toluene layer, leaving behind a colorless aqueous solution. The same procedure is followed for the preparation of dodecylamine-stabilized Ag, Pt and Ru nanoparticles, except $AuCl_3$ being replaced by $AgNO_3$, H_2PtCl_6 and $RuCl_3$.

2.1.1. Preparation of gold nanoparticles

Generally, gold nanoparticles are produced in a liquid ("liquid chemical methods") by reduction of chloroauric acid ($H[AuCl_4]$), although more advanced and precise methods do exist. After dissolving $H[AuCl_4]$, the solution is rapidly stirred along with the addition of a reducing agent that converts Au^{3+} to Au^0. With the formation of more and more gold atoms, the solution becomes supersaturated, that leads to precipitation in the form of sub-nanometer particles. The rest of the gold atoms that form stick to the existing particles and if the solution is stirred vigorously, the particles will be fairly uniform in size.

To prevent the particles from aggregation, a stabilizing agent that could stick to the nanoparticle surface is usually added. The prepared nanoparticles are functionalized with various organic ligands to create organic-inorganic hybrids with advanced functionality [17]. Santanu Bhattacharya synthesized gold nanoparticles by dissolving 5 mg of $HAuCl_4{\cdot}3H_2O$ in methanol followed by the addition of 5 mg $NaBH_4$. The mixture was then bath-sonicated for 5 min to ensure proper mixing of Au and $NaBH_4$. The reduction of Au^{3+} to Au^0 was achieved by using 15-fold excess of $NaBH_4$. Immediate colour change from bright yellow to red was observed. Red precipitation was noticed within a minute after the addition of reducing agent. The supernatant was removed and the precipitate was washed twice with

water and MeOH each to remove the impurities. The nanoparticles were designated as Au-1. Bhandari and Sharma used preparation of simultaneous TBP self assembled threads and TBP-capped gold nanoparticles for which 0.6 mL of cold freshly prepared 0.1 M $NaBH_4$ aqueous solution was added to 20 mL 0.25 mM $HAuCl_4$ aqueous solution and the solution was kept under stirring condition for at least 12 hours at 30 °C. The temperature was precisely maintained by circulating thermostated water within the uncertainties of ±0.01 °C. The solution was then transferred to 10 mL tightly capped sample tubes and kept for aging in dark for 1 month. Similar reactions were carried out at 40, 50, and 60 °C. In each case, a light pink color appeared initially with different color intensities at different temperatures. The color slowly disappeared on aging within 4-5 days leading to the appearance of black threads floating at the bottom of the sample tube. Afterwards the nature of the solution remained essentially the same for several months. Zhao and Xu chose gold as a core for Au-Pt core-shell nanoparticles because its surface favors deposition of platinum and shows inertness in acid electrolytes [18,19]. Brown and coworkers synthesized gold nanoparticles of diameter ranging from 2.6 to 100 nm, using a seeding technique. They compared the use of citrate and hydroxylamine as reductant. The citrate seeded particles were highly uniform in size; however, the hydroxylamine seeded gold colloids produced two distinct populations of large spheres and small rods [20]. It was found that the 2.6 nm diameter seeds had a standard deviation of ~1 nm. The citrate method which is one of the best-known methods for producing gold nanoparticles that involves reduction of $HAuCl_4$ by sodium citrate was first developed by Turkevich *et al.* [17]. Brust synthesized thiol-derivatized gold nanoparticles of 1-3 nm diameter in a two-phase liquid-liquid system. Sodium borohydride was used for the reduction of $AuCl_4$ in the presence of alkanethiol [21]. Yang and coworkers used a combination of seeding growth and digestive ripening for achieving precise control of monodispersed gold nanoparticles. Alkyl amines were used for the stabilization and thermal reduction of $HAuCl_4$. Gold nanoparticles of various diameters (2.1-8.8 nm) were produced. A change in color of the sol was noticed. The sol was brown for particles of 2.1 nm and red for 3.1 nm [22]. In polyol method AuNP-PEG-A solution is prepared by mixing 0.2 mM aqueous solution of thiolated poly ethylene-glycol (PEG) with AuNP-H_2O system. A solution of AuNP-PEG-B is prepared by mixing 0.2 mM aqueous solution of PEG with AuNP-citrate solution. The method is preferred over other processes because of fewer chances of impurities and role of ethylene glycol as a solvent as will as a reducing agent.

2.1.2. Preparation of silver nanoparticles

For the preparation of silver nanoparticles 300 mg of $AgNO_3$ is added to 180 cm^3 of ethanol at a temperature of 60 °C with constant stirring. Different aminosilanes are dissolved in ethylene glycol followed by dispersion in alcohol-$AgNO_3$ solution previously prepared under stirring to obtain $AgNO_3$ aminosilanes in various ratios. Maribel and coworkers synthesized silver nanoparticles using two stabilizing agents, sodium dodecyl sulphate (SDS) and sodium citrate [23]. Silver nitrate solution (1.0 – 6.0 mM) was used as metal salt precursor. Hydrazine hydrate solution with a concentration of 2.0 - 12 mM and sodium citrate solution (1.0 - 2.0 mM) were used as reducing agents. Sodium citrate was also used as stabilizing agent at room temperature. The transparent colorless solution was converted to the characteristic pale yellow color which indicated the formation of silver nanoparticles. These were then purified by centrifugation. For the removal of excess silver ions, the silver colloids were washed thrice with deionized water under nitrogen stream. A dried powder of the nanosize silver was obtained by freeze-drying. The most convenient method of synthesizing Ag nanoparticles is polyol process in which the mixture of 3 mL each of 1.0 mM $AgNO_3$ solution (prepared in ethylene glycol) and PVP is kept for 45 minutes in oven at 175 °C. The appearance of blackish brown color shows the formation of Ag nanoparticles.

2.1.3. Preparation of platinum nanoparticles

Stable aqueous colloidal platinum nanoparticles are prepared by citrate reduction. The method was first used by Furlong who prepared platinum nanoparticles as small as 4 nm [17]. It was found that increasing heat during the reaction causes an increase in particle size. Henglein *et al*. produced different Pt colloidal sols by utilizing radiolysis, hydrogen and citrate reduction [24]. Particles with average diameter of 1.8, 2.5, and 7.0 nm are obtained by Radiolysis, citrate and hydrogen reduction. The citrate acts not only as a reductant, but also as a stabiliser for Pt colloidal sols [19]. Lin *et al*. shaped citrate-stabilised platinum nanoparticles of 2-3 nm average size, with approximately ±2 nm distribution

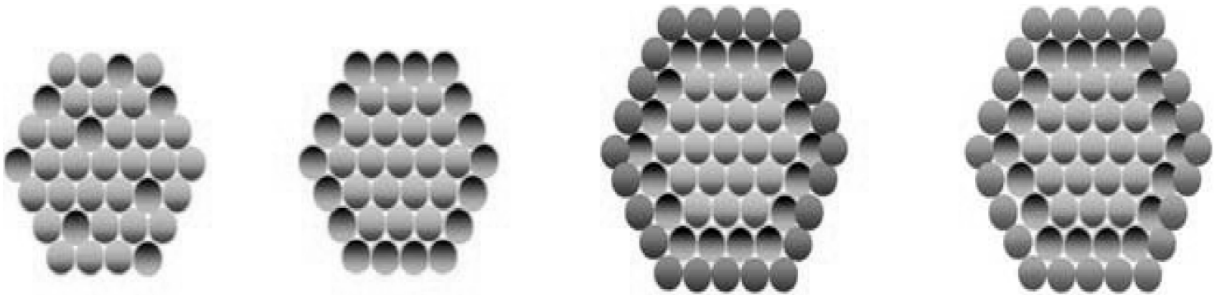

Fig. 1. Different structures of bimetallic nanoparticles.

via methanol reduction. Luo and Sum devised a single-step heat-treatment method for the production of poly(vinylalcohol) (PVA) stabilised platinum nanoparticles with diameters of 2-7 nm. The PVA acted as reductant and stabiliser [20].

2.1.4. Preparation of ruthenium nanoparticles

Vladimir and his team synthesized 20 wt.% Ru/C under argon using dry solvents [25]. In a 2-L two-neck flask fitted with a dropping funnel and a vacuum adapter, maintained under a steady flow of argon, 2.868 g of anhydrous ruthenium chloride and 1 L of dry THF were introduced and sonicated for 15 min to generate a uniform suspension of the salt. 5.6 g of vulcan XC 72 was added to the suspension, and the mixture was stirred vigorously for 2 h at room temperature. The flask was then placed in an oil bath maintained at 50 °C. 27.0 mL of 1.5 M LiBet3H/ THF solution was dripped over 2 h, and the resulting mass was allowed to stir vigorously for 24 h at 50 °C. After stopping the stirring the flask was allowed to cool to room temperature. Colorless and clear supernatant was pressed off and the precipitate was washed twice with 150 mL portions of THF and dried. The residue was conditioned at 200 °C using argon (5 min) followed by hydrogen (30 min) and argon (5 min) again. The sample tube was allowed to cool to room temperature. This enabled the formation of stable, 20 wt.% Ru/C catalyst.

2.2. Bimetallic nanoparticles (BMNP)

BMNP are the combination of two metals in the nanoscale size range. This area of nanoscience is gaining mounting attention in the field of catalysis due to synergistic effects. BMNP have four types of mixing patterns: core-shell nanoparticles, sub-cluster nanoparticles, mixed (alloy) nanoparticles and multishell nanoparticles. Core-shell nanoparticles consist of a shell of one type of atom surrounding a core of another type of atom as shown in Fig. 1 [26].

Supriya Devarajan used *N,N*-[3-(trimethoxysilyl)propyl]diethylenetriamine (TPDT), tetraethoxysilane (TEOS), chloroauric acid, palladium chloride, silver nitrate, chloroplatinic acid, sodium borohydride, and methanol for the preparation of different structures of bimetallic nanoparticles [26]. Double-distilled water was used in Brust process. Ethylene glycol was used as a solvent in case of polyol process.

2.2.1. Preparation of bimetallic nanoparticles

Burst *et al.* added 130 μl of *N,N*_-[3 (trimethoxysilyl)propyl]diethylenetriamine (TPDT) to 3.8 ml of methanol followed by 50 μl H_2O and 50 μl 0.1 M HCl. [26] The mixture was shaken well for a couple of minutes. Different volumes of 0.01 M $AuCl_3$, $AgNO_3$, H_2PtCl_6, and $RuCl_3$ were added to the silica sol and mixed well until the solution became homogeneous. Sodium borohydride (2.5 mg) was then added with vigorous stirring. Instantaneous color change ranging from deep violet of Au colloid to brown color of Ru and Pt or yellowish brown in case of Ag colloid, depending on the composition, was observed. Various molar compositions of the two metal components such as 0.25:0.75, 0.43:0.57, 0.5:0.5, 0.57:0.43, 0.75:0.25, and 0.9:0.1 were prepared using the same protocol. The sols and the resulting solid monoliths of all the compositions were very stable over extended periods of several months.

Films of different thickness ranging from 0.1 to 10 μm were cast on glass slides by a coating process. Gels and monoliths of any desired shape were obtained by allowing the solvent to evaporate. The dried material was found to shrink considerably but slow evaporation of the solvent led to crack the free monoliths.

2.2.2. Preparation of Au-Ag bimetallic alloy nanoparticles

Sang W. Han prepared nanoparticles via the two-phase method [21]. Initially, aqueous solutions of

potassium tetrachloroaurate ($KAuCl_4$), potassium dicyanoargentate ($KAg(CN)_2$) and their mixtures in various molar ratios of $AuCl_4$ /AgCN were prepared; the total solute concentration was chosen to be the same in all solutions, i.e., 40 mM. Into a beaker, 30 mL of one of these aqueous solutions and 50 mL of 50 mM tetraoctylammonium bromide in toluene were added together, and the resulting immiscible mixture was stirred vigorously until all of the $AuCl_4$ and AgCN species in aqueous phase were transferred into the organic layer. 0.2 mL of neat dodecanethiol was added to the organic phase and subsequently a freshly prepared aqueous solution of 0.4 M sodium borohydride (25 mL) was added with vigorous stirring. After the mixture was stirred further for 12 h, the organic phase was separated and evaporated to 10-20 mL in a rotary evaporator. The resulting solution was mixed with 300 mL of ethanol to remove excess thiol and then kept in a refrigerator at 218 °C for 6 h. Thereafter, the dark brown precipitate was filtered and washed with ethanol and acetone. The synthesized particles were characterized by UV-Vis and Infrared spectroscopy. Supriya Devarajan and coworkers used tetraoctylammonium bromide (TOABr) and sodium mercaptopropionate (Na-MPA). Solutions of Na-MPA were aged for 3-5 days before the experiment [27]. Initially, water (95 mL) containing desired mole fractions of Au and Ag (total metal concentration was maintained at 2.94×10^{-4} M) was refluxed and a required amount of Na- MPA (147 μL of 0.1 M resulting in 1.47×10^{-4} M) and 5 mL of 1% aqueous trisodium citrate solution were added simultaneously. The color of the solution changed from turbid yellow to varying shades of reddish-brown depending on the alloy composition. The sol was boiled for another hour and then cooled to room temperature. Various compositions with different mole fractions of Au and Ag were prepared.

In phase-transfer experiments two immiscible layers were obtained by mixing 50 ml toluene containing 3.88×10^{-4} M TOABr with 50 ml of hydrosol containing alloy nanoparticles. Initially, the aqueous layer at the bottom was colored and the organic phase was colorless. This biphasic mixture was vigorously stirred and a transfer of the alloy nanoparticles from aqueous to toluene phase was observed by the movement of color across the interface. The organic phase was collected and the solvent was rotary-evaporated to yield a brown colored powder which was washed thoroughly with ethanol to remove the uncoordinated TOABr.

Au-Ag alloy nanoparticles were also synthesized by the reduction of $HAuCl_4$ and $AgNO_3$ with $NaBH_4$ in the presence of sodium citrate [27]. For ensuring complete solubility of Ag^+ in the presence of Cl^- the solutions used in Au and Ag seed preparation were diluted by a factor of 50 in order to lower the reaction quotient (Q) to 2.5×10^{-11} [28]. Flasks were cleaned with aqua regia and deionized water and then filled with 100 mL of deionized water and 50 L of 0.01 M sodium citrate. Varying mole fractions of 0.01 M $HAuCl_4$ and 0.01 M $AgNO_3$ were added to each solution for a total metal salt concentration of 10 M. The solution was allowed to stir for an additional 30 s. A faint color change occurred almost immediately. The color change caused by the reduction of metal salts was found to be dependent on the concentrations of $AgNO_3$ and $HAuCl_4$ in solution. The pure Ag solution turned from colorless to light yellow upon addition of $NaBH_4$. In contrast, the 75%Ag/25%Au solution turned yellowish red. As the Au/Ag molar ratio increased, the intensity of the reddish color increased. In the first method AgCN used is poisonous so it should be replaced by $AgNO_3$. PVP can also be used because it is the best solvent as will as reducing agent.

2.2.3. Preparation of the Au-Pt bimetallic nanoparticles

Hau and Shu prepared Au-Pt nanoparticles by adding the reductant into the solution containing 0.2 mM $AuCl_4$ and varying concentration of $PtCl_6^{-2}$ (0.2-0.8 mM). The reductant was a solution of 4 mL tannic acid (2%) and 1 mL citric acid (1%). The reaction mixture was stirred for 15 min at 100 °C, followed by 10 min of stirring without heating [28]. Schrinner and his team used cationic spherical polyelectrolyte brushes carrying chains of poly(2-aminoethylmethacrylate hydrochloride) [29]. The radius of the core particles was 45 nm and the average contour length of the grafted chains was 165 nm. The entire number of charged groups in the polyelectrolyte layer was determined precisely by conductometric titration [29]. Another research team successfully deposited platinum onto gold nanoparticles by reducing $K_2[PtCl_6]$ with hydrogen in a colloidal solution of gold nanoparticles with a narrow size distribution (10 nm ±1.2 nm), in the presence of PVP as stabilizer [30]. Kumar and Zou prepared colloidal gold of 3 nm diameter using 3-aminopropyltrimethoxysilane for the attachment of colloidal gold to ITO glass slides via surface derivatization. Platinum films were deposited on to the colloidal gold by means of the galvanic replacement technique [31,32]. Henglein produced Au(core)-Pt(shell) and Pt(core)-Au(shell) bimetallic nanoparticles using hydrogen reduction and radiolysis techniques.

2.2.4. Production of Au-Ru bimetallic nanoparticles

The research group of Akita shaped Au(core)-Ru(shell) bimetallic nanoparticles with a diameter of 13±3.2 nm via a sonochemical technique [33]. The product nanoparticles were recovered by centrifugation and washed with ethanol several times to remove nonspecifically bound dodecylamine. The nanoparticles were then dried at room temperature in vacuum.

The synthesis of Au-Ru core-shell nanoparticles by sequential polyol process involves the reduction of $Ru(acac)_3$ (acac = acetylacetonate) in refluxing glycol using PVP stabilizer. The resulting Ru nanoparticles (mean particle size = 3.0 nm) are subsequently coated with Au by adding $AuCl_3$ to the Ru/glycol colloid and slowly heating to 200 °C. The Au-Ru alloy nanoparticles can also be synthesized via co-reduction of the $[Ru(CO)_3Cl_2]_2$ dimer and $Au(acac)_3$ with glycol at 200 °C. Monometallic Au and Ru nanoparticles are prepared from $AuCl_3$ and $Ru(acac)_3$, respectively, using slight modifications of published procedures [34].

3. CHARACTERIZATION

The sol-gel derived silicates containing nanoparticles are very stable in both liquid and solid phases. The stability is checked by following the absorbance spectra over extended periods of several months. The amino groups present in the silicate stabilize the BMNP as proposed by Lev and co-workers [35,36]. The use of sodium borohydride results in fast reduction of metal ions. But ethylene glycol is the best reducing agent and stabilizer that also acts as a solvent. A variety of techniques such as UV-Visible spectroscopy, TEM, XRD, FTIR, and CV are used for the characterization of nanoparticles.

3.1. Au-Ag Bimetallic alloy nanoparticles

3.1.1. UV-visible studies

Fig. 2 shows the absorption spectra of different compositions of Au and Ag (0.57:0.43, 0.43:0.57, and 0.25:0.75 molar ratios). Alloy formation is evidenced by the appearance of a single peak with λ_{max} depending strongly on composition. The plasmon band is blue-shifted with increasing amount of silver [37,38]. The absorption spectra of Au, Ag, and Au-Ag alloy nanoparticles of varying mole fractions show a linear relationship between the λ_{max} and Au mole fraction (Fig. 2). A physical mixture of

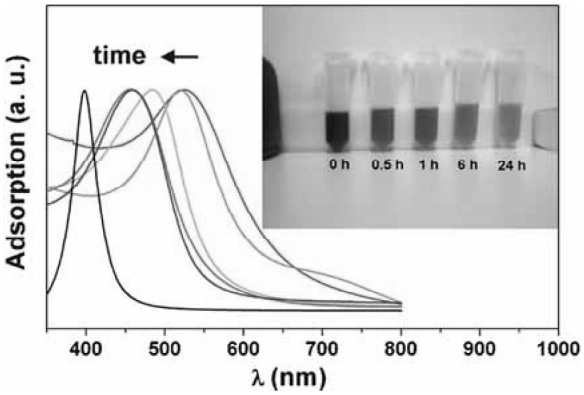

Fig. 2. UV-visible spectra of Au-Ag nanoparticles.

the individual colloids, however, shows two surface plasmon peaks corresponding to the monometallic counterparts. The stability of the silver colloids in the silicate matrix, however, is very low. This could be attributed in part to the low stability constant of the Ag-amine complex [39,40]. This is subsequently revealed in the relative instability of Au-Ag alloys where the Ag content is higher than 50%. The formation of bimetallic dispersions depends on the kinetics and thermodynamics of reduction of individual components. The complete reduction of Au(III) and Ag(I), under the present conditions requires 5 and 10 min, respectively. The stability value for Au is expected to be close to that of silver based on the ease of reduction as observed in the time required for complete formation of the metallic colloid. Hence, it is expected that Pd and Pt may form a shell, while Au may occupy the core of the bimetal in case of Au-Pd and Au-Pt bimetallic structures. However, from CO adsorption measurements, it is observed that both the metals are present with an enrichment of Pt and Pd on the surface. In the case of Au-Ag bimetal, silver enrichment is observed. It is reported that planar Au-Ag alloys formed by high-temperature method exhibit an enrichment of Ag on the surface, due to

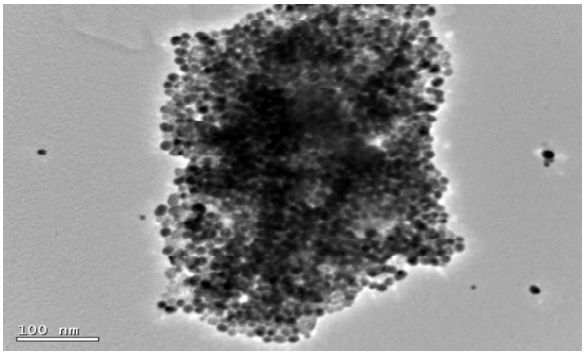

Fig. 3. TEM images of Au-Ag Alloy nanoparticles.

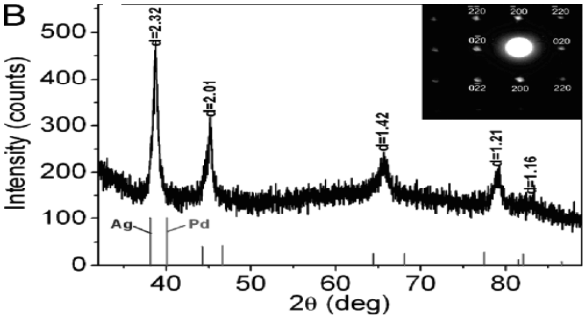

Fig. 4. XRD spectra of Au-Ag nanoparticles.

lower heat of sublimation of Ag than Au [41,42]. However, in case of nanoparticles preparation under ambient conditions, the borohydride reduction and the metal atom deposition chemistry may play a role in determining the surface enrichment. It is found that the use of only tetraethoxysilane or methyltrimethoxysilane or trimethylamine as the stabilizer results in the precipitation of the particles. This suggests a dual role for the aminosilanes as stabilizers of nanobimetallic particles. It is possible that the amino groups stabilize the nanobimetallic particles while the –Si–O–Si– and Si–OH form a network surrounding the metallic particles.

Additionally, the use of long-alkyl-chain-containing matrices is expected to help in the stabilization of nanoparticles by keeping them far apart and thereby preventing coagulation. Mulvaney and coworkers [43,44] have reported the formation of silica shells around gold nanoparticles prepared using silanes. Lev and his team [45,46] postulated that silanes form a network around the nanometallic particles of gold, silver, platinum, and palladium. The stability of the mono- as well as the bimetallic colloidal dispersions is found to be very good and the particle size does not change with time. Absorbance of the sol as well as the dry gel is found to be indistinguishable immediately after preparation and after several months of storage. The particle size distribution is retained in both solid and liquid phases. It is observed that the absorbance spectra of a silicate film (3-μm thickness) containing bimetallic nanoparticles of composition 1:1 molar ratio of the salts is nearly the same as that of the sol. In this case, the film is formed from a mixture of TPDT and TEOS. The addition of TEOS to the sol decreases the cross-linking time but does not change the absorbance spectra.

3.1.2. TEM studies

Au-Ag alloy particle size ranges from 1 to 6 nm with the maximum close to 2.5 nm as can be seen from the histogram in Fig. 3. The lattice spacing obtained from the HRTEM is 2.30 ± 0.01 Å. There is no lattice mismatch observed since the Au and Ag have very similar lattice parameters.

3.1.3. XRD studies

As mentioned in the introduction, Au and Ag have very similar lattice constants and hence their *d* and 2θ values lie very close to each other. Fig. 4 shows the XRD spectra corresponding to the Au-Ag alloy. The molar ratio of silane to metal salt is maintained at 100:5, using 1:1 Au to Ag ratio. As for the diffractogram of Ag, the strongest band is observed at 38.14° (2θ) that corresponds to the (111) plane. A broad band is observed at 44.15° (2θ) that can be attributed to the (200) crystallographic plane. Two broad reflections are observed at 64.55° and 77.48° (2θ) that correspond to the (220) and (311) planes [47]. In the case of the Au–Ag alloy all reflections are similar to monometallic Au and Ag. The particle size is calculated to be 5 ± 1 nm based on the (111) peak, which corroborates well with the data obtained from TEM.

3.1.4. CO adsorption studies

Gold and silver have fully occupied *d*-orbitals and exhibit weak coordination ability toward CO [47,48]. It is reported that only weak Raman and IR bands are observed for CO on gold and silver surfaces to be adsorbed [48].

3.2. Au-Pt Bimetallic alloy nanoparticles

3.2.1. UV-visible spectroscopy

The UV-Vis spectra of Au-Pt sol are very similar to those of Au-Ru sol. Fig. 5 shows comparison between the UV-Vis spectra of different compositions of Au and Pt (0.75:0.25, 0.5:0.5, and 0.25:0.75 molar ratios of $HAuCl_4$:H_2PtCl_6) and the monometals. The molar ratio of silane to metal ion is 100:0.25. This is less than the corresponding ratios used for other systems. It is known that Au and Pt tend to precipitate when mixed together at high concentrations of Pt [11]. The Pt sol is brown and shows a broad absorption band. The absence of peaks at 378 and 460 nm indicates the reduction of Pt(IV). In case of physical mixtures, the plasmon remains visible for all ratios of Au and Pt.

3.2.2. TEM studies of Au-Pt alloy nanoparticles

The size of Au-Pt bimetallic particle varies between 1 and 6 nm. Fig. 6 shows the HRTEM of the

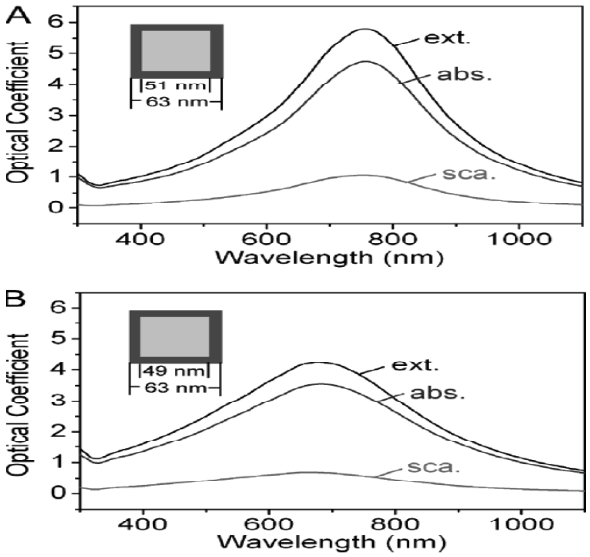

Fig. 5. UV-visible spectroscopy of Au-Pt alloy nanoparticles at various concentrations.

bimetallic particles. The lattice is quite well-resolved and equally spaced showing the single crystalline nature of the nanoparticle. The lattice spacing is 2.30 ± 0.01 Å. Bulk Pt has a lattice spacing of 2.27 Å. Assuming Vegard's law, the observed lattice spacing will yield a nominal composition of 1:2 Au/Pt for a starting composition of 5:1 Au/Pt [49]. This value should be treated with some caution since even a small variation in the measurement of the lattice spacing could lead to a large error in the final composition.

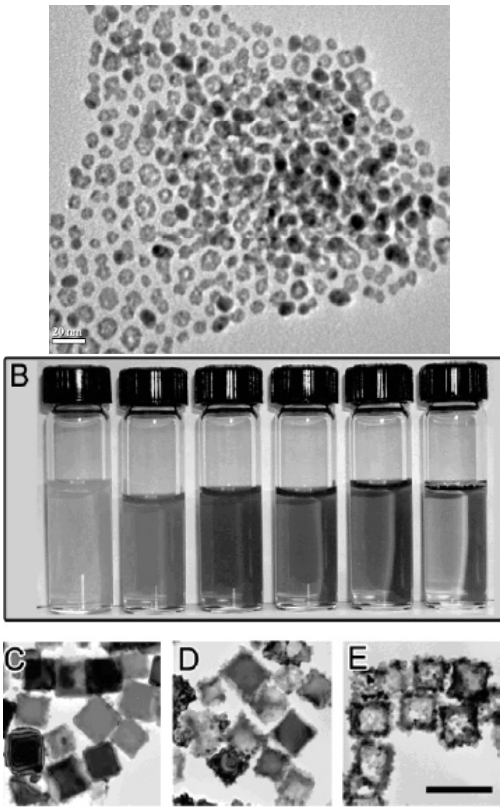

Fig. 6. TEM images of Au-Pt Alloy nanoparticles.

3.2.3. XRD studies

The molar ratio of silane to metal salt and Au to Pt is maintained at 100:5 and 5:1 in order to avoid precipitation. Pt, like Pd is more crystalline than gold nanoclusters in silicate matrices. Fig. 7 indicates that the (200) band observed at 45.44° (2θ) is very sharp. A strong band at 56.47° (2θ) may be due to the (102) reflection of PtO_2. Bands are also observed at 65.94° (2θ) and 75.22° (2θ) that correspond to the (111) and (201) planes of PtO_2, respectively. The XPS data of the bimetal also shows Pt in oxidized states [50].

The Au-Pt bimetal exhibits a broad band at 38.35° (2θ) that matches with the (111) plane A broad peak at 44.58° (2θ) is attributed to the (200) plane. Two additional bands are observed at 65° and 77.73° (2θ) that correspond to PtO_2 (JCPDS 38-1355). The particle size calculated on the base of (111) peak is 7 ± 1 nm which is close to the value observed by TEM measurements.

3.2.4. CO adsorption Studies

The IR spectrum of CO adsorbed on TPDT-stabilized Au-Pt particles show a strong band at 2030 cm^{-1} and is assigned to the linearly adsorbed CO on the Pt surface [51]. Hence, in both Au-Pd and Au-Pt bimetallic particles, an enrichment of Pd and Pt is observed on the surface.

3.3. Au-Ru bimetallic alloy nanoparticles

3.3.1. TEM studies

The Au-Ru nanoparticles show a mean particle size of 4.1 nm (Fig. 8a), which is larger than that of monometallic Ru nanoparticles (3.0 nm) and smaller than that of monometallic Ru nanoparticles (6.1 nm) [52,53]. The high-resolution transmission electron microscopy (HRTEM) image in the inset shows a typical Au-Ru nanoparticle with (111) lattice fringes. The TEM image (Fig. 8c) of the assembled system indeed shows large extended aggregate structures consisting of two different types of particles (core-shell Ag-Pt and core-shell Au-Ru nanoparticles) with good repeatability, of which, the core-shell Ag-Pt nanoparticles can be easily identified by the strong image contrast between the core and shell components. The core-shell Au-Ru nanoparticles

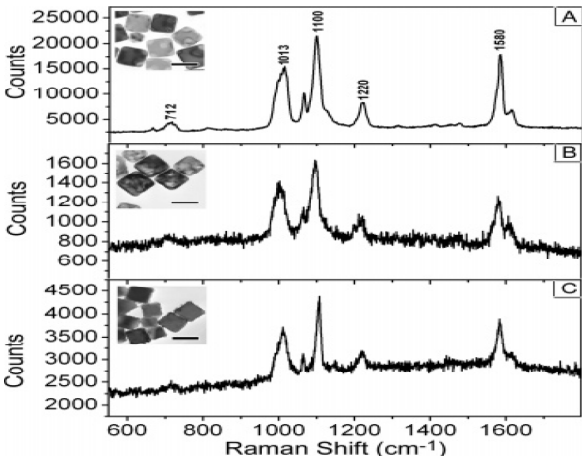

Fig. 7. XRD patterns of Pt, PtAu(1:1), and AuRu(1:1) nanoparticles (from bottom to top) deposited on MWNT–IL film.

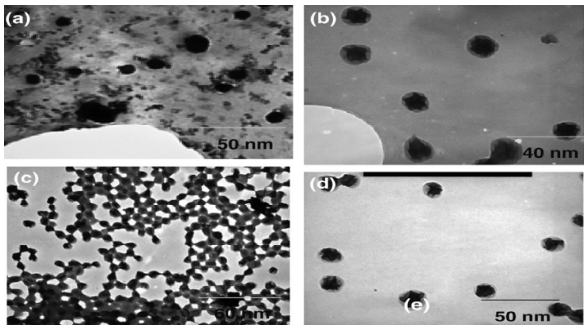

Fig. 8. TEM image of Au-Ru alloy nanoparticles.

were nearly alternating with each other in the assembly, and forming three dimensional structures on the TEM grid. On the contrary no isolated particles were found on the TEM grid.

TEM image of mixture of core-shell Ag-Pt and Au-Ru nanoparticles functionalized by non-complementary thiolated oligonucleotides.

3.2.2. XRD studies

The diffractograms of the bimetallic combinations generally show broad bands while their monometallic counterparts exhibit fairly sharp bands [54,55]. The particle sizes of the bimetallic combinations determined from the XRD spectra correlate well with the sizes obtained from TEM measurements. The particle size is calculated on the base of Debye Scherrer equation:

$$D_p = 0.9\lambda / \beta \cos\theta, \qquad (1)$$

where D_p corresponds to the particle size in Å, λ is the Xray wavelength, θ is the Bragg angle, and β corresponds to the full width at half maximum (fwhm, in radians) of the peak under consideration. When the samples are heated to 200 °C for 3 h, the peaks

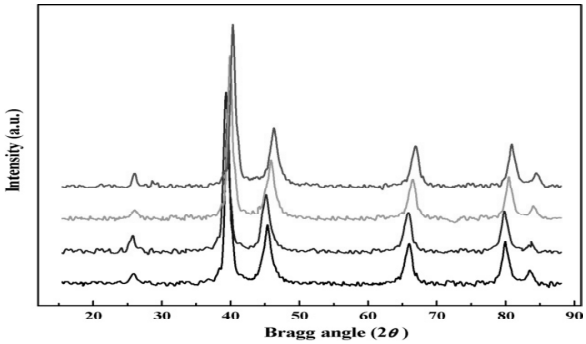

Fig. 9. XRD studies of Au-Ru alloy nanoparticles.

become well-defined and sharp due to increased crystallinity as shown in Fig. 9. On heat treatment the particle size increases threefold for all bimetallic combinations [56-58].

The XRD spectra of the monometals as well as the bimetal of different compositions have been recorded for the as-prepared samples in the form of dry powders. The molar ratio of silane to metal salt is maintained at 100:5 [59]. As for the monometals, it is observed that Ru is more crystalline than the gold nanoclusters in silicate matrices. The peak that appears at around 38° (2θ) corresponds to the (111) crystallographic plane and the peak at around 45° (2θ) corresponds to the (200) plane (JCPDS 4-0784, 5-0681). The diffractograms show that (111) crystallographic surface is marked for gold clusters (2θ = 38.46°) and is broad, while the (200) plane is less distinct (2θ = 44.41°). Two additional broad bands are observed at 64.48% (2θ) and 77.71° (2θ) and they correspond to the (220) and (311) planes of Au, respectively.

In the case of Ru, there is a strong band at 56.33° (2θ), which closely matches the (222) plane. This is not surprising since it is known that Ru gets oxidized fairly fast when under ambient conditions [60-62]. Another strong band is seen at 45.37° (2θ), which corresponds to the (200) plane of Ru. The observed reflections for the bimetal clusters are slightly different from that of the monometallic components. The (111) plane is observed at 38.62° (2θ) and the (200) plane occurs at a value of 45.25° (2θ) for the bimetal of Au-Ru molar ratio 1:1 Fig. 9. These values lie in between the values reported for monometallic clusters. The particle size has been calculated (using Eq. (1)) to be 4 ± 1 nm based on the (111) peak. These values are close to the values deduced from TEM measurements. A fairly strong band is seen at 66.2° (2θ), which lies close to the (400) reflection of RuO [63]. Two sharp bands are seen at 75.34° (2θ) and 75.15° (2θ) in Au–Ru bimetal and Ru, respectively.

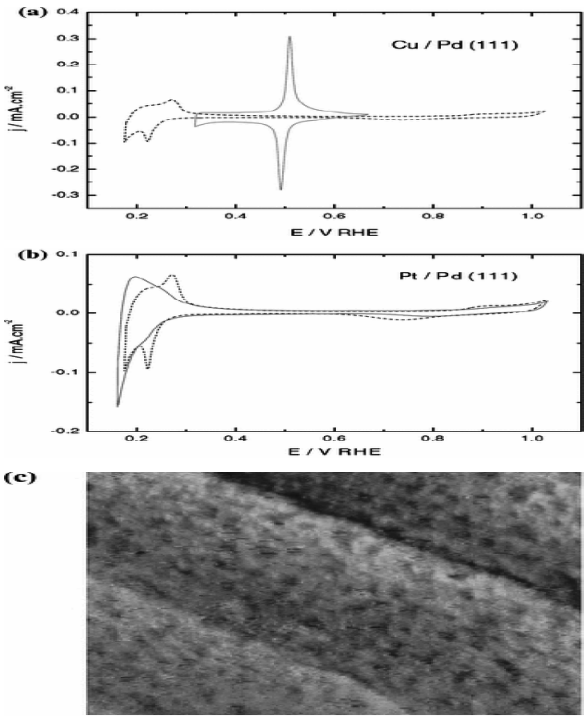

Fig. 10. Cyclic voltammograms and AFM image of PtRu(1:1)/GCE, PtRu(1:1)–MWNT/ GCE, and PtRu(1:1)–MWNT–IL/GCE in 0.5 M H_2SO_4 solutions.

3.3.3. CO adsorption studies

Infrared spectroscopy has been widely used to study the surface chemistry of small, adsorbed molecules [64]. The vibrational frequency of adsorbed CO changes with the metal substrate and binding structure. Hence, IR spectroscopy of CO on the surface of bimetallic nanoparticles is expected to give information about the surface of the nanoparticle. On gold nanoparticles, however, CO is known to be very weakly and reversibly adsorbed. The adsorbed CO is generally observed only at low temperatures for Au-Ru [65].

3.3. Electrochemical studies

The electrocatalytic activity of the nanoparticles stabilized in silicate matrices has been followed by carrying out preliminary studies on Au-Ag, Au-Pt and Au-Ru alloy nanoparticles. A glassy carbon electrode coated with silicate stabilized nanoparticles has been used. Oxygen reduction is taken as the demonstrative case. Use of TEOS along with TPDT to stabilize the particles facilitates cross-linking and the resulting films are found to be very sturdy and adherent to the substrate. Cyclic voltammetric experiments have been performed on the modified electrode in phosphate buffer pH 7.2. Fig. 10 shows the cyclic voltammograms on the bare as well as nanometal modified electrodes. It is clear that the oxygen reduction potential shifts to more positive values in presence of the metallic particles. A potential shift of about 200 mV in the case of Au-Ru modified classy carbon electrode Fig. 11 shows the catalytic nature of the immobilized metallic particles [66-68].

3.4. FT-IR studies

FT-IR studies have been carried out to follow the evolution of silicate matrix during the stabilization of the metallic particles. The spectra have been taken for the dried material and they represent the completely polymerized silicate network

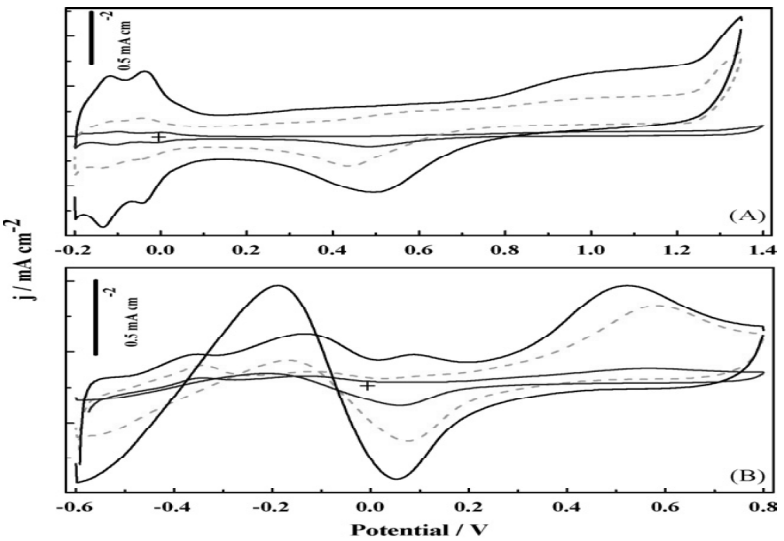

Fig. 11. CV of a PtRu(1:1)–MWNT–IL/GCE in PBS (pH 7.4) containing 10 mM glucose. Multiple anodic peaks attributed to the oxidation of glucose and resulting intermediates are observed for the positive scan.

encapsulating the nanoparticles. The IR peaks agree well with the reported literature values [66] for silicate matrices. The band at 1117 cm^{-1} confirms the presence of siloxane groups [γ(Si–O–Si)] in the polymerized material while the band at around 1659 cm^{-1} corresponds to the primary amine [$\delta(NH_2)$] of the silane. The position of this band shifts to higher values as the silane is cross-linked and polymerized. The N–H stretching band around 3500 cm^{-1} is broadened in the cross-linked material as compared to that of neat silane. This is attributed to the complexation of the amine groups of the silicate with the metal particles [66].

4. APPLICATIONS OF BIMETALLIC ALLOY NANOPARTICLES

4.1. Electrical conductivity

Among metal fillers, Ag flakes are most widely used because Ag has the highest electrical conductivity and, unlike many other metals, their oxides have relatively better conductivity [69-71]. However, there have been some concerns on the electromigration of Ag ions in the Ag filled adhesives in the presence of high humidity and electrical bias. Thus, other low cost metal i.e., copper has been proposed as alternate conductive filler in electrically conductive polymer composites for the next generation, due to its high electrical conductivity, low electrical migration, and high compatibility with the next generation of Cu interconnect technology. However, due to its facile oxidation, the existence of pure copper is difficult and its generation from Cu-salt requires complete inertness. A thin layer of silver coating on copper particles has been an approach to improve the electrical and physical performance of copper fillers. Conductive polymer composites filled with these silver coated copper fillers (~5 μm) have shown considerably high electrical conductivity [72]. Another solution is the formation of Ag-Cu alloy. A similar approach (i.e., alloying of Au with Ag) can improve the use of Au as an electrode material by decreasing its inertness [73].

4.2. Electroplating and fabrication

For fabricating the silver coated gold particles, Ag coating process such as electroplating is required. Moreover, current commercial silver-gold particles have micron-size, which are larger than the required size, will not be suitable for ultra-fine pitch (<100 nm) assembly. Thus, a simpler fabricating method and finer particles i.e., in nanosize are necessary for the low cost manufacturing and fine pitch applications. Bimetallic alloy nanoparticles properties are influenced by both metals and show more advantages over ordinary metallic NPs [74,75]. They offer tunability in the sense that the metal composition and structures of nanoparticles can be varied to optimize the nanostructure properties. Bimetallic alloy nanoparticles have shown activities as catalysts in chemical reactions and in environmental remediation. The interest in bimetallic nanoparticles as MEMS switch lubricants includes controlled Nanotexturing and the ability to tailor contact behavior using desirable properties of each metal involved. Microelectromechanical systems (MEMS) (also written as Micro Electro Mechanical or microelectronic and Microelectromechanical systems) is the technology of very small mechanical devices driven by electricity; it merges at the nano-scale into Nanoelectromechanical systems (NEMS) and nanotechnology. Nanotexturing was proved to be beneficial for MEMS switch contacts using bimetallic nanoparticles [76,77]. Metal alloys of Au with Ag, Cu, Pt, or Pd were found to have decreased wear as compared to pure Au contacts at the expense of higher cost [78-80]. Bimetallic nanoparticles allow more than one metal to be used in the contact without the expense and complexity of integrating and Au alloy into the MEMS switch fabrication process.

4.3. Reduction in electromigration and electronics behaviors

Among the variety of bimetallic nanoparticles, Ag-Au Nanoparticles have been investigated as a candidate material for electrode or interconnection lines in flexible electronics, since Ag films have a lower resistivity (1.63 Ω) and melting point (961.8^{0}C) than other metal films. Nevertheless, pure Ag lines are liable to induce system failure resulting from the electromigration of ions, which is one of the main reliability issues in modern integrated circuits. It is reported in refs. [81-83] that the alloying of Cu into Ag reduces the electromigration. Interconnection lines composed of Ag nanoparticles or Ag–Cu alloy nanoparticles fabricated on poly (ether sulfone) (PES) substrates have been prepared. Moreover, their electrical characteristics have been investigated with and without optical heating [84]. Nano sized Au/Ru alloy particles synthesized in the polymer matrix have overcome the fine pitch interconnection and simplified surface mounting technology [85,86].

4.4. Plasmonic and electromagnetic enhancement

An important application of bimetallic nanoparticles is their development as substrates (hosts) capable of providing large electromagnetic enhancements for surface enhanced spectroscopy [86,87]. Such enhanced local field properties originates as a result of surface plasmon resonance (SPR) due to collaborative oscillations of the free conduction band electrons on the metal surface on resonant excitation with electromagnetic radiation [88,89]. The surface plasmon enhanced luminescence observed in bimetallic nanoparticles have currently captured exponential attention due to their relevance as color displays, optical amplifiers as well as optical sensors [90,91].

4.5. Unusual optical and electrical properties

The unusual optical and electrical properties of bimetallic nanoparticles arise due to several factors like modification of the electronic structure of bimetallic nanoparticles like Au-Pt, interplay between volume and surface properties, chemical reactions between the nanoclusters and interparticle interactions [90,92]. However, fabrication of nano scale monometallic and particularly inter-metallic particles encapsulated within dielectric (glasses) matrices are not simple and encounter several difficulties like different chemical reactivity of two metals with the matrix, which can promote separation (via oxidation, for instance) instead of alloying of the species.

4.6. Potential applications

Bimetallic alloy nanoparticles embedded in surfaces regions of glass are of great interest because of their potential application [93,94]. Specific linear and nonlinear optical properties have been achieved for Ag-Au alloy nanoparticles in silica glasses [95]. The resulting macroscopic properties are based on a surface plasmon resonance (SPR), the frequency of which depends strongly on the materials (types of metals) and their composition.

4.7. Thermal conductivity

Nanofluids, consisting of bimetallic nanoparticles suspended in a heat-transfer liquid, may offer significant enhancement of thermal conductivity, which is technologically important for cooling applications that rely on the efficient transfer of heat.

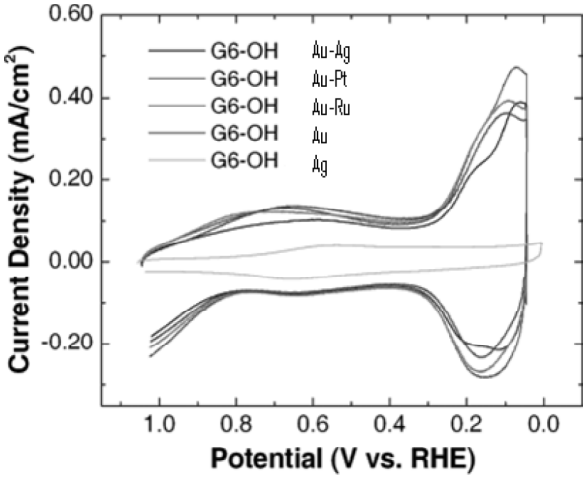

Fig. 12. Typical cyclic voltammograms of the methanol oxidation with different bimetallic nanoparticle catalysts in 2 M CH_3OH and 1 M H_2SO_4 under deoxygenated conditions. The scan rate was 60 mV/s.

This is a problem that affects such diverse facets of industry as ventilation systems, automotives, cooling towers, and chemical process plants. It has been demonstrated that nanofluids consisting of Ag-Au in water enhances the thermal conductivity of the fluids [96,97]. Additionally, thermal conductivity of nanofluids has been associated with strong temperature dependence [98,99] and a significantly higher critical heat flux than that of the pure fluid [100].

Electron transport in nanostructures, particularly in bimetallic nanoparticles and their arrays is not only of academic interest, but also holds promise in nanoelectronics [101,102]. Synthesis of bimetallic alloy nanoparticles and nanowires of desired properties, therefore, assumes countless significance for the developing world.

4.8. Electrocatalytic activities

Among the platinum based catalysts, Pt-Ru is currently the most promising anode catalyst for the oxidation of methanol in low temperature direct methanol fuel cells, Bimetallic systems prepared by the assembly method linking the Pt and Ru nanoparticles by a biomolecule (e.g. DNA), have been explored for applications in catalysis [103]. The catalytic performance of these bimetallic Pt-Ru aggregates (actually core-shell Ag-Pt and Au-Ru aggregates) in methanol electro-oxidation has been evaluated by cyclic voltammetry. The results were intended to provide interesting insights into the difference between alloy nanoparticle catalysts and

Table 1. Comparison of the electrochemical activities of the catalysts.

Nanoparticles	onset potential (mV versus NHE)	forwardpeak potential (mVversus NHE)	forwardpeak current (A/mgofPt)	I_f/I_b current ratio (efficiency)
Au-Ag	411	913	0.68	2.95
Pt-Au	409	892	0.052	2.34
Ru-Au	431	887	0.10	2.50
Au	351	898	0.033	2.33
Ag	424	899	0.031	2.30

the ensemble of constituent monometallic nanoparticles [104].

Electrocatalytic activities of the MWCNT-supported bimetallic nanoparticles for the oxidation of methanol were examined using CV (Fig. 12). The voltammograms consist of two oxidation peaks: one in the forward scan (arrow left to right) and the other in the backward scan. It was observed that the oxidation of the Aurium and bimetallic surfaces occurred during the forward scan when the switching potential exceeded 1.1 V versus NHE, and during the backward scan, the reduction peak was observed at around 0.7-0.8 V versus NHE. Hence, the CV was conducted within the potential range of 1.1 and 0.3 V versus NHE. As seen in Fig. 12, backward scans do not contain the oxidation/ reduction peak of platinum or the secondary metals. The forward scan is attributable to methanol oxidation, forming Au-adsorbed carbonaceous intermediates, including carbon monoxide (reaction 2) and CO_2 (reaction 3). This adsorbed carbon monoxide (CO_{ads}) causes the loss of activity of the electrocatalyst. [105,106].

$$Pt + CH_3OH \rightarrow Pt\text{-}CO_{ads} + 4H^+ + 4e^-, \quad (2)$$

$$CH_3OH + H_2O \rightarrow CO_2 + 6H^+ + 6e^-, \quad (3)$$

The backward oxidation peak, shown as reaction (4), is attributed to the additional oxidation of the adsorbed carbonaceous species to carbon dioxide [56].

$$Pt\text{-}CO_{ads} + H_2O \rightarrow Pt + CO_2 + 2H^+ + 2e^-. \quad (4)$$

Therefore, the current ratio of the forward scan peak current (I_f) over the backward scan peak current (I_b) shows the amount of methanol oxidized to carbon dioxide relative to carbon monoxide [107,108]. A higher I_f/I_b value suggests that the catalysts are more efficient at lowering the adsorbed carbon monoxide. The current ratio is a useful way of comparing the long-term catalytic activity between the different catalysts. Previous investigators have conducted a chronoamperometric along with a CV studies and demonstrated that catalysts with a higher I_f/I_b ratio are correlated with catalyst longevity [109,110] The MWCNT-supported bimetallic nanoparticle catalysts all exhibit at least 60% higher I_f/I_b ratio relative to that of Au and Ag monometallic nanoparticles (I_f/I_b = 1.4). It is interesting to note that the Au-Ru bimetallic system has a high I_f/I_b ratio (2.50) next to that of the Pt-Au system [111,112]. Table 1 summarizes the onset potentials, the forward peak potentials, the forward peak current, and the current ratio (I_f/I_b) of each bimetallic electrocatalyst. The onset potential suggests the apparent activation energy of methanol oxidation. All of the Pt-based bimetallic catalysts have a lower onset potential than that of the Pt monometallic catalyst, with the onset potential of Au being the lowest.

Gold nanoparticles are of high interest as a potential core for bimetallic core-shell nanoparticles, as they are easy to synthesize and more economically viable than the metals that are generally used for catalysis. Platinum nanoparticles have been extensively studied for their catalytic properties [113] as Pt is a highly useful industrial catalyst for reducing automobile pollutant gases, for producing hydrogen from methane and in the direct methanol fuel cell electrochemistry, electrocatalysis, and fuel cells.

5. CONCLUSIONS

The preparation of various bimetallic nanoparticles in organically modified silicates has been demonstrated. The citrate-stabilized gold nanoparticle seeds acted as better starting material for the bimetallic core-shell nanoparticles; but suffered problems with aggregation and morphology. The thiol-stabilised gold nanoparticles were of improved morphology, but that made coating of gold nanoparticles difficult. Stabilization by PVP was preferred as it was free of the above disadvantages. The detailed discussion on Au-Ru and Au-Pt

bimetallic particles revealed that the surface consisted of both metals while Au-Ag formed alloy phases. The sols remain stable for several months and can be handled and characterized easily. However, XRD measurements carried out on dried samples indicated the formation of oxides since sol-gel based silicates are known to be highly porous and permeable to oxygen. The XRD studies also revealed that the nanobimetallic particles predominantly assemble in fcc structure. The results indicated that vapor phase synthesis (solvated metal atom dispersion method) leads to nanoparticles assembling in hcp structure. The method employed for the synthesis of the particles seems to play important role in determining the packing behavior. It appears that fcc ordering is preferred by single crystalline particles while polycrystalline particles follow hcp packing. XRD and TEM measurements for aminosilicatestabilized bimetallic particles indicate clear single crystalline behavior. The bimetallic particles prepared by the sol-gel method have been shown to electrocatalyze the reduction of oxygen. The synthesized bimetallic alloy nanoparticles can be successfully applied in nanoelectronics, fuel cells, optical amplifiers and sensors.

ACKNOWLEDGEMENT

The authors gratefully acknowledge Quaid-i-Azam University and Higher Education Commission Islamabad, Pakistan, for providing financial assistance.

REFERENCES

[1] P. R. Couchman and W. A. Jesser // *J. Nat. Products* **269** (2000) 481.
[2] A. Ceylan, K. Jastrzembski and S. I. Shah // *Metallurgical and Materials Transactions A*. **37** (2006) 2033.
[3] N. Toshima and Y. Wang // *Adv. Mater.* **6** (2000) 240.
[4] N. Toshima and P. Lu // *Chem. Lett.* **25** (2001) 725.
[5] J. H. Kim, A. S. Ishihara, N. Mitsushima and K. I. Kamiya // *Electrochim. Acta* **52** (2007) 2492.
[6] B. Wang // *J. Power Sources* **152** (2005) 1.
[7] V. M. Jalan and E. J. Taylor // *J. Electrochem. Soc.* **130** (2000) 2299.
[8] B. C. Beard and P. N. Ross // *J. Electrochem. Soc.* **137** (2001) 336.
[9] S. Mukerjee, S. Srinivasan, M. P. Soriaga and J. McBreen // *J. Electrochem. Soc.* **142** (1995) 1409.
[10] T. Toda, H. Igarashi, H.Uchida and M. Watanabe // *J. Electrochem. Soc.* **146** (2000) 3750.
[11] E. Antolini, J.R.C. Salgado, L.G.R.A. Aantos, G. Garcia, E.A. Ticianelli, E. Pastor and E.R. Gonzalez // *J. App. Electrochem.* **36** (2006) 355.
[12] S. Remita, G. Picq, J. Khatouri and M. Mostafavi // *Radiation Physics and Chemistry* **54** (2000) 463.
[13] C. S.Lin, M. R. Khan and S. D. Lin // *J. Colloid and Interface Sci.* **299** (2006) 678.
[14] Z. Y. Li, J. P. Wilcoxon, F. Yin , Y. Chen , R. E. Palmer and R. L. Johnston // *Faraday Discuss.***138** (2008) 363.
[15] K. R. Brown, D.G. Walter and M. J. Natan // *Chem Mater.* **12** (2000) 306.
[16] Y. Yang, Y. Yan and W. Wang // *J. Nanotechnology* **19** (2008) 7.
[17] J. Turkevich and G. Kim // *J. Nanotech.* **169** (2000) 873.
[18] A. Voevodin // *J. Appl. Phys*. **3** (2007) 1950.
[19] M. Mrozek and F. Y. M. Xie // *J. Anal. Chem.* **73** (2001) 5953.
[20] K.R. Brown, L. Lyon, A.P. Fox, B.D. Reiss and M.J. Natan // *Chem. Mater.* **12** (2000) 314.
[21] S.W. Han, Y. Kim and K. Kim // *J. Colloid Interface Sci.* **208** (1998) 272.
[22] C. Ziegler and A. E. ller // *J. Phys. Chem. C.* **115** (2011) 4502.
[23] H. Rehman, M. Springborg and Y. Dong // *J. Phys. Chem. A.* **115** (2011) 2005.
[24] D. Zhao and B. Q. Xu // *Angew. Chem. Int. Ed.* **45** (2006) 4955.
[25] M. B. Mohamed, Z. L. Wang and M.A. El-Sayed // *J. Phys. Chem.* **103** (2001) 10255.
[26] J .Turkevich, P.C. Stevenson and J. Hillier // *Discussion of the Faraday Soc.* **11** (1951) 55.
[27] S. Devarajan, B. Vimalan and S. Sampath // *Journal of Colloid and Interface Sci.* **278** (2004) 126.
[28] M.P. Mallin and C.J. Murphy // *Nano Letters* **2** (2002) 1235.
[29] M. Schrinner, F. Polzer, Y. Mei, Y. B. Lu, M. Haupt, A. Ballauff, G. ldel and M. Drechsler // *Macromol. Chem. Phys.* **208** (2007) 1542.

[30] Y. Mizukoshi, T. Fujimoto, Y. Nagata, R. Oshima and Y. Maeda // *J. Phys.Chem. B* **104** (2000) 6028.
[31] N. Toshima, M. Harada, T. Yonezawa, K. Kushihashi and K. Asakura // *J. Phys. Chem.* **95** (2001) 7448.
[32] R. J. Davis and M. Boudart // *J. Phys. Chem.* **98** (2002) 5471.
[33] A. Henglein // *Langmuir* **15** (2000) 6738.
[34] R.S. Liu, H.M. Chen and S.F. Hu // *China Particuology* **2** (2004) 160.
[35] D.Q. Lu, Q.K. Tong and C.P. Wong // *IEEE Transactions on Components and Packaging Technology* **22** (1999) 360.
[36] J. Hongjin, C. P. Kyoung-sik-Moon // *Wong School of Materials Science and Engineering and Packaging Research Center (Georgia Institute of Technology, Atlanta, GA*) **20** (2005) 30332.
[37] L.R.P. Kassab, C.B. de Araújo, R.A. Kobayashi, R.D. de A Pinto and D.M. da Silva // *J. Appl. Phys.* **102** (2007) 1035.
[38] L.R.P. Kassab, F.A. Bomfim, J.R. Martinelli, N.U. Wetter, J.J. Neto and C.B. de Araújo // *J. Appl. Phys. B* **94** (2009) 239.
[39] T.H. Tsai, S.H. Wang and S.M. Chen // *Journal of Electroanal. Chem.* **659** (2011) 69.
[40] D.Q. Lu, C.P. Wong and Q.K. Tong // *IEEE Transactions on Components and Packaging Technology* **20** (2000) 250.
[41] D.Q. Lu, Q.K. Tong and C.P. Wong // *IEEE Transactions on Components and Packaging Technology* **22** (2001) 360.
[42] T. Som and B. Karmakar // *J. Lumin.* **128** (2008) 1989.
[43] D.R.C. Lide, *Handbook of Chemistry and Physics* (Boca Raton, 1998).
[44] K. Terashima, T. Hashimoto, T. Uchino, S.H. Kim and T. Yoko // *J. Ceram. Soc. Jpn.* **104** (1996) 1008.
[45] W. Vogel, *Handbook of Glass Chemistry* (Springer-verlag, Berlin, 1992).
[46] O. Stranik, H.M. McEvoy, C. McDonagh and B.D. MacCraith, *Plasmonic enhancement of fluorescence for sensor applications* (Berlin, 2005).
[47] R.A.J. Coutu, P.E. Kladitis, K.D. Leedy, R.L.J. Crane and M. Micromech // *J. Appl. Phys.* **97** (2005) 94300.
[48] S. Morita, R. Wiesendanger and E. Meyer, *Noncontact Atomic Force Microscopy. 1st ed. Nanoscience and Technology* (Springer Series, 2002).
[49] L. Xiong and A. Manthiram // *J. Electrochem. Soc.* **152** (2005) 697.
[50] M.L. Wu, D.H. Chen and T.C. Huang // *Chem. Mater.* **13** (2001) 599.
[51] M.L. Wu, D.H. Chen and T.C. Huang // *J. Colloid Interface Sci.* **243** (2001) 102.
[52] Z. Liu, X.Y. Ling, X. Su and J.Y. Lee // *J. Phys. Chem. B* **108** (2004) 8234.
[53] D. Chu and S.Gilman // *J. Electrochem. Soc.* **143** (2000) 1685.
[54] A. Cabanas, D. P. Long and J. Watkins // *J. Chem. Mater.* **16** (2004) 2028.
[55] T. Yonezawa and N. Toshima // *J. Chem. Soc. Faraday Trans.* **91** (2000) 4111.
[56] F. Xiao, F. Zhao, D. Mei, Z. Mo and B. Zhang // *Biosens. Bioelectron* **24** (2009) 3481.
[57] J. Huang, Z. Liu, C. He and L.M. Gan // *J. Phys. Chem. B* **109** (2005) 16644.
[58] G. Hoogers, *Fuel Cell Technology Handbook* (CRC Press, Boca Raton, 2003).
[59] R. Manoharan and J. B. Goodenough // *J. Mater. Chem.* **2** (2000) 875.
[60] T. Iwasita, H. Hoster, A. John-Anacker, W.F. Lin and W. Vielstich // *Langmuir* **16** (2000) 522.
[61] T. Page, R. Johnson, J. Hormes, S. Noding and B. Rambabu // *J. Electroanal. Chem.* **485** (2000) 34.
[62] J. Prabhuram, T.S. Zhao, Z.K. Tang, R. Chen and Z.X. Liang // *J. Phys. Chem. B* **110** (2006) 5245.
[63] J. Lipkowski and P.N. Ross, *Electrocatalysis* (Wiley-VCH, New York, 1998).
[64] S. Mukerjee, S. Srinivasan and M. Soriaga // *J. Phys. Chem.* **99** (2000) 4577.
[65] L. Xiong, A.M. Kannan and A. Manthiram // *Electrochem. Commun.* **4** (2002) 898.
[66] S. Mukerjee, S. Srinivasan, M.P. Soriaga and J. McBreen // *J. Electrochem. Soc.* **142** (2000) 898.
[67] G. Tamizhmani and G.A. Capuano // *J. Electrochem. Soc.* **141** (2000) 968.
[68] T. Toda, H. Igarashi, H. Uchida and M. Watanabe // *J. Electrochem. Soc.* **146** (1999) 3750.
[69] E. Antolini, R.R. Passos and E.A. Ticianelli // *Electrochim Acta* **48** (2002) 263.
[70] D.Q. Lu, C.P. Wong and Q.K. Tong, In: *1998 International Symposium on Advanced Packaging Materials*.
[71] Y. Junggwon, C. Kyoungah, P. Byoungjun, K. Ho-Chul, J. Byeong-Kwon and K.J. Sangsig // *J. of Appl. Phys.* **47** (2008) 5070.

[72] S. Koh, F. T. Michael and P. Strasser // *Electrochim. Acta* **52** (2007) 2765.
[73] C. Sanchari, R. Venkat, D. Bhethanabotla and S. Rajan // *J. Phys. Chem. C* **113** (2009) 13016.
[74] M. Mohl, D. Dobo, A. Kukovecz, Z. Konya, K. Kordas, J. Wei, R. Vajtai and P.M. Ajayan // *J. Phys. Chem. C* **115** (2011) 9403.
[75] Q. Huang, H. Yang, Y. Tang, T. Lu and D.L. Akins // *Electrochem. Commun.* **8** (2006) 1220.
[76] M. P. Mallin and C. Murphy // *J. Nano Lett.* **2** (2002) 1235.
[77] W. Aiqin, H.Y. Ping, C.Y. Fan and M.C.Yuan // *J. Catalysis* **237** (2006) 197.
[78] L. Xiong and A. Manthiram // *Electrochim. Acta* **50** (2005) 2323.
[79] K.I. Johnson and D.V. Keller // *J. App. Phys.* **38** (2009) 1896.
[80] H.J. Jiang, K. Moon and C.P. Wong, In: *Proc. Int. Symp. On Advanced Packaging Materials: Processes, Properties and Interfaces.*
[81] L. Xiong and A. Manthiram // *J. Electrochem. Soc.* **152** (2005) 697.
[82] M.A. Shah and A. Towkeer, *Principles of Nanoscience and Nanotechnology* (Narosa Publishing House, New Dehli, 2010).
[83] G. Rowe, T.H. Jones and P.N. Walls // *J. Public Understanding of Science* **14** (2005) 333.
[84] J. Luo, N. Kariuki, L. Han, L. Wang, C.J. Zhong and T. He // *Electrochim. Acta* **51** (2006) 4821.
[85] R.B. Andrew, A.C. Michael, A.S. Dietram, R.S. Bret and A.C. Elizabeth // *Public Understanding of Science* (2010) 1.
[86] C. Sonnichsen, S. Geier, N.E. Hecker, G. Von-Plessen, J.H. Feldmann, B. Ditlbacher, J.R. Lamprecht, F.R. Krenn, V.Z.H. Aussenegg, J.P. Chan and M.M. Spatz // *Appl. Phys. Lett.* **77** (2000) 2945.
[87] N. Travitsky, T. Ripenbein, D. Golodnitsky, Y. Rosenberg, L. Burshtein and E. Peled // *J. Power Sources* **161** (2006) 782
[88] J. C. Avies, *Nanotechnology Oversight: An Agenda for the Next Administration* (Washington, DC, 2008).
[89] D.A. Skoog, F.J. Holler and S.R. Crouch, *Principles of Instrumental Analysis, 6th ed. (*Thomson Higher Education, Belmont, CA, 2007).
[90] A. Stassi, C.D. Urso, V. Baglio, A.D. Blasi, V. Antonucci, A.S. Arico, A.M. Catroluna, A. Bonesi and W.E. Triaca // *J. Applied Electrochemistry* **36** (2006) 1143.
[91] G. Raschke, S. Kowarik, T. Franzl, C. Sönnichsen, T. A. Klar, J. Feldmann, A. Nichtl and K. Kurzinger // *Nano Letters* **3** (2003) 935.
[92] C. Sonnichsen, S. Geier, N.E. Hecker, G. Von-Plessen, J.H. Feldmann, B. Ditlbacher, J.R. Lamprecht, F.R. Krenn, V.Z.H. Aussenegg, J.P. Chan, and M.M. Spatz // *Appl. Phys. Lett.* **77** (2000) 2945.
[93] J.H. Kim, A. Ishihara, S. Mitsushima, N. Kamiya and K.I. Ota // *Electrochim. Acta* **52** (2007) 2492.
[94] G.P. Wiederrecht // *Eur. Phys. J. Appl. Phys.* **28** (2004) 3.
[95] H. Ditlbacher, J.R. Krenn, B. Lamprecht, A. Leitner and F.R. Aussenegg // *Opt. Lett.* **25** (2000) 560.
[96] H. Zhong, H. Zhang, G. Liu, Y. Liang and B. Hu // *J. Electrochem. Commun.* **8** (2006) 707.
[97] M. Salerno, J.R. Krenn, B. Lamprecht, G. Schider, H. Ditlbacher, N. Felidj, A.L. Felidj and F. Aussenegg // *Opto-Electron. Rev.* **10** (2002) 215.
[98] W.L. Barnes, A. Dereux and E.T.W. Dereux // *Nature* **424** (2003) 820.
[99] B. Wang // *J. Power Sources* **152** (2005) 1.
[100] J.E. Avron, G. Bisker, D. Gershoni, N.H. Lindner and E.A. Meirom // *Phys. Rev. Lett.* **100** (2008) 120501.
[101] T. Kalkbrenner, M. Ramstein, J. Mlynek and V.Sandoghdar // *J. Microsc.* **202** (2001) 70.
[102] V.M. Jalan and E.J. Taylor // *J. Electrochem. Soc.* **130** (1999) 2299.
[103] R.B.P. Elmes, K.N. Orange, S.M. Cloonan, D.C. Williams and T. Gunnlaugsson // *J. Am. Chem. Soc. **133** (*2011) *15862*.
[104] W. Lu, *Nanowire based electronics: Challenges and prospects,*(IEEE International, USA, 2009).
[105] A.R. West, *Solid State Chemistry and Its Applications* (Wiley, New York, 1984).
[106] D.A. Schultz // *Curr. Opin. Biotechnol.* **14** (2003) 136.
[107] J.R. Lombardi, R.L. Birke, T.H. Lu and J. Xu // *J. Phys. Chem.* **84** (1986) 4174.
[108] U.A. Paulus, T.J. Schmidt, H.A. Gasteiger and R.J. Behm // *J. Electroanal. Chem.* **495** (2001) 134.

[109] F.H.B. Lima, M.J. Giz and E.A. Ticianelli // *J. Braz. Chem. Soc.* **16** (2005) 328.
[110] C.F. Bohren and D.R. Huffman, *Absorption and Scattering of Light by Small Particles* (New York, 1998).
[111] L.G.R.A. Santos, C.H.F. Oliveira, I.R. Moraes and E.A. Ticianelli // *J. Electroanal. Chem.* **596** (2006) 141.
[112] T. Ressler // *J. Phys. IV* **C2 7** (2000) 269.
[113] J. Prabhuram, T.S. Zhao, Z.K. Tang, R. Chen and Z.X. Liang // *J. Phys. Chem. B* **110** (2006) 5245.